ELSEVIER

Journal of Non-Crystalline Solids 217 (1997) 250–263

JOURNAL OF
NON-CRYSTALLINE SOLIDS

Vitreous silica bulk and surface self-diffusion analysis by molecular dynamics

David A. Litton, Stephen H. Garofalini *

Department of Ceramics and Interfacial Molecular Science Laboratory, Rutgers University, PO Box 909, Piscataway, NJ 08855, USA

Received 18 March 1996; revised 24 February 1997

Abstract

Molecular dynamics simulation was used to investigate the kinetics of self-diffusion in the bulk and on the surface of pristine vitreous silica. Multibody potential functions were used to describe interatomic forces. Activation energies were found to be similar for Si and O self-diffusion and did not vary appreciably between self-diffusion in the bulk and on the surface. For both species in the bulk and on the surface, average activation energies ranged from 113–115 kcal/mol. Oxygen self-diffusivity was found to be only slightly higher than silicon self-diffusivity in the bulk and on the surface. Self-diffusion coefficients in the top 3–7 Å of the surface were found to be higher than those of bulk simulations by less than a factor of two. Self-diffusion on the surface was observed to occur by motion of SiO_3 and SiO_4 polyhedra over several angstroms while bulk self-diffusion involved significant neighbor exchange over similar length scales. Surface diffusion through a vapor phase (via desorption and re-adsorption at a distant location on the surface) was not included in the surface data. © 1997 Elsevier Science B.V.

1. Introduction

The technological significance of vitreous silica (v-SiO_2) is wide-ranging. Applications in optical elements, such as dielectric layers in microelectronics, and as catalyst supports have stimulated many investigations of this material. The presence of thin amorphous silica layers on the surfaces of silicon carbide and silicon nitride materials affects the properties of powders and polycrystalline products. For all of these technologies, the transport properties of v-SiO_2 play an important role in process control and ultimate properties. For high surface area applications, an understanding of the relative roles of bulk and surface diffusion is essential.

Bulk self-diffusion of oxygen in vitreous silica has been measured by or inferred from several techniques, as reviewed by Lamkin et al. [1]. The majority of the work done in this area involved ^{18}O tracer exchange between silica samples and oxygen gas in contact with them. Diffusion coefficients were calculated from the changes in concentration profiles over time. These concentration profiles were generated using non-resonant nuclear reaction analysis (NRA) or SIMS [2–9]. The data from these vapor phase exchange techniques are difficult to interpret since both interstitial and network diffusion occur simultaneously and may interact. Mikkelsen [10] calculated self-diffusivity of network oxygen from SIMS (secondary ion mass spectroscopy) concentration profiles

* Corresponding author. Tel.: +1-908 445 2216; fax: +1-908 445 4655; e-mail: shg@rutile.rutgers.edu.

0022-3093/97/$17.00 © 1997 Elsevier Science B.V. All rights reserved.
PII S0022-3093(97)00107-5

of chemically deposited Si $^{16}O_2$–Si$^{18}O_2$ thin film couples. Brebec et al. [11] determined the self-diffusion coefficients for Si in SiO_2 by depositing ^{30}Si enriched silica films on fused quartz substrates and analysing concentration changes via SIMS. Viscosity measurements of several commercial grades of v-SiO_2 by fiber elongation have been reported by Hetherington et al. [12].

Although much work has been reported on surface diffusivity of adsorbates on single crystals using FIM (field ion microscopy), PEEM (photoemission electron microscopy) and LID (laser induced desorption) [13,14], these techniques are not suitable for measuring surface self-diffusivities of amorphous materials. The advent of surface probe techniques such as STM (scanning tunneling microscopy), AFM (atomic force microscopy) and NSOM (near-field scanning optical microscopy) may provide a means for such measurements, though none were found in the literature.

Several investigators have used the molecular dynamics (MD) computer simulation technique to model bulk vitreous silica [15–24] or the fluoride analog, BeF_2 [25,26]. By applying an interatomic potential to a system of atoms and solving Newton's classical equations of motion iteratively, a time evolution of the atomic positions and thermodynamic properties of the system are generated. Whereas experimental techniques yield data averaged over large numbers of atoms and long times, MD simulations allow atomic-scale interpretations of observed phenomena. In the earliest cases, the interatomic potentials used in these studies were simple ionic pair potentials [16,18–21]. However newer potentials incorporate multibody potentials to account for the partial covalency of v-SiO_2 [15,17,22,23,27,28]. In each case, the model glasses reproduced the structure predicted by the continuous random network model (CRN), with the corners of SiO_4 tetrahedra connected by bridging oxygen atoms. Good matches of Si–O, O–O and Si–Si model PDFs with experimental data were seen, with reasonable bond angle distributions. The inclusion of three-body potentials improved the match of model bond angle distributions with diffraction data [15].

The MD technique has also been used to model the vitreous silica surface in vacuum and in the presence of water vapor [27–29]. The outermost surface of the dry model glass was oxygen-rich, containing non-bridging oxygens (NBO) and strained siloxane bonds, as observed in experiment. The near-surface region of the dry model glass contained two-, three- and four-membered rings, as well as under- and over-coordinated species. Surfaces formed in the presence of water vapor contained fewer topological and bonding defects and a silanol (≡SiOH) concentration in close agreement with experiment [28].

The MD technique provides a means to study bulk and surface self-diffusion in v-SiO_2 on the atomic level. Since the motions of individual atoms can be tracked, diffusion coefficients can be calculated. Diffusive mechanisms can be observed using computer graphics. Several simulated bulk glass self-diffusion coefficients and mechanisms have been previously reported [17,19–21,25,26,30]. A comparison between surface and bulk self-diffusion coefficients for glasses simulated using only pair potentials has been previously reported [30]. The purpose of the present work is to compare surface and bulk self-diffusion coefficients of v-SiO_2 simulated using three body potentials [15]. Results for bulk simulations will be compared with experimental and MD simulation results. Diffusive mechanisms for each type of system will be discussed.

The potentials and an outline of the MD technique and diffusion analysis procedure are discussed in Section 2.

2. Computational procedure

The pair and three-body potentials and parameters used in the present work are described elsewhere [15]. Modified Born–Mayer–Huggins (BMH) ionic potential functions are used for the Si–Si, Si–O, and O–O pair interactions,

$$v_2(\boldsymbol{r}_i, \boldsymbol{r}_j) = v^{\mathrm{BMH}}(r_{ij}) = A_{ij} \exp(-r_{ij}/\rho_{ij}) + Z_i Z_j \operatorname{erfc}(r_{ij}/\beta_{ij})/r_{ij}, \quad (1)$$

where $r_{ij} = |\boldsymbol{r}_i - \boldsymbol{r}_j|$, Z_i is the formal ionic charge and A, ρ and β are parameters. In this modification of the BMH pair potential, screening effects and lack of complete charge transfer are taken into account empirically by the complementary error function term.

Three-body interactions of the form

$$v_3(\boldsymbol{r}_i, \boldsymbol{r}_j, \boldsymbol{r}_k) = h_3(r_{ij}, r_{ik}, \theta_{jik}) + h_3(r_{jk}, r_{ji}, \theta_{kji}) + h_3(r_{ki}, r_{kj}, \theta_{ikj}), \quad (2)$$

where

$$h_3(r_{ij}, r_{ik}, \theta_{ijk}) = \lambda_{jik} \exp\{\gamma_{ij}/(r_{ij} - r_{ij}^0) + \gamma_{ik}/(r_{ik} - r_{ik}^0)\} \times \{\cos(\theta_{jik}) - \cos(\theta_{jik}^0)\}^2, \text{ for } r_{ij} < r_{ij}^0, \quad (3a)$$

and

$$h_3(r_{ij}, r_{ik}, \theta_{ijk}) = 0 \text{ otherwise}. \quad (3b)$$

with θ_{jik} as the angle subtended by r_{ij} and r_{ik} with the vertex at i, were used to describe the directional dependent bonding in O–Si–O and Si–O–Si configurations. This potential increases the energy of the system whenever the angle formed by a central atom and two of its covalently bonded neighbors varies from the preferred angle, θ^0. This preferred angle for O–Si–O and Si–O–Si configurations is the tetrahedral angle ($\theta^0 = 109.5°$), although the three-body term is quite weak for the latter configuration. The three-body term contributes less than 1% to the total energy of bulk v-SiO_2 [15].

Diffusion was analyzed for two bulk silica systems and three silica surfaces with no silanols (pristine). As discussed elsewhere [27], the MD melt-quench technique was used to form the bulk system and the systems from which the various surfaces were formed, using a quench rate of 2×10^{13} K/s to cool from 5000 to 300 K. The original bulk systems contained 648 atoms in a (21.4 Å)^3 cubic MD cell. All bulk simulations were performed within the microcanonical ensemble, using periodic boundary conditions (pbc) in the x, y and z directions to avoid end effects. The Nordsieck–Gear predictor–corrector algorithm was employed to integrate Newton's $3N$ equations with a time step of 1 fs. The glass structure simulated by this technique was in reasonable agreement with that determined by X-ray and neutron diffraction experiments [15,31].

To simulate glass surfaces, the periodic boundary conditions in the z direction were removed and atoms in the bottom half of the MD cell (with respect to the z direction) were frozen as previously discussed [27]. As discussed above, structure and the concentrations of topological defects in the simulated surface systems were consistent with experiment [27,28]. The starting configurations for diffusion analysis runs consisted of two bulk v-SiO_2 systems and three pristine surface systems containing 648 atoms at 300 K. Each of these configurations was then heated to 4800, 5000, 5200, 5600, 6000, 6400, 6800 and 7200 K for 100 ps at each temperature. During the first 10 ps of these runs the temperature was kept constant by velocity rescaling. Velocities were then rescaled whenever the system temperature deviated from the setpoint by more than 100 K for the remaining 90 ps to avoid temperature drift over the long simulation times. A time step of 0.25 fs was used and configurations were saved every 0.25 ps, for a total of 400 configurations. For surface systems, the reflecting boundary was maintained at 10 Å above the surface, such that any atoms that desorbed from the surface could get well beyond the interaction cutoff of 5.5 Å before being reflected back toward the surface.

Diffusion was analyzed over the final 90 ps, thus the final 360 configurations of each run. For the bulk systems, mean squared displacement, $\bar{r}^2$, was calculated over all possible elapsed times. Thus, the first 359 configurations were each considered the initial configuration, t_0, and squared displacement was summed for all Si and O atoms for each configuration after t_0 to the end of the run. Mean squared displacement was then averaged over all squared displacements over a given elapsed time for each atom type. The diffusion coefficient was then calculated from the slope of $\bar{r}^2$ as a function of elapsed time,

$$D = \frac{\bar{r}^2}{2\alpha t}, \quad (4)$$

where α equals the dimensionality of the diffusion. For bulk diffusion, α was 3, while for surface difference we used values of both 2 (for 2D diffusion) and 3 (3D diffusion).

For surface systems, only the atoms on the surface were considered when calculating the diffusion coefficient. This was accomplished by counting only atoms with z-coordinates greater than a specified value, thus creating a volume of specific thickness

parallel to the surface. Each configuration having a given atom in the specified surface volume was considered t_0 for all consecutive configurations ($t_0 + \Delta t$) for which that atom remained within the surface volume. Atoms which desorbed to > 5.5 Å above the surface were not summed.

Activation energies for diffusion, Q, and diffusivity pre-exponential factors, D_0, were calculated using regression analysis of D as a function of reciprocal temperature, $1/T$,

$$D = D_0 \exp(-Q/RT). \quad (5)$$

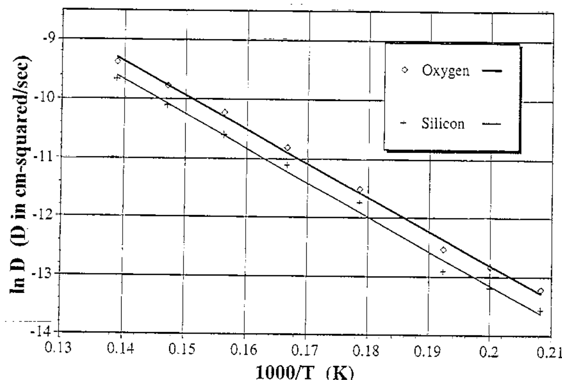

Fig. 2. Arrhenius plot of the natural log of D as a function of reciprocal temperature for both species in bulk silica simulations.

3. Results

3.1. Bulk diffusion

Mean-squared displacement, $\bar{r}^2$, is plotted as a function of elapsed time, Δt, for both Si and O ions in the 6000 K bulk model glass in Fig. 1. As discussed above, the diffusion coefficient at this temperature is calculated from the slope of these curves. The inset expands the short time region of the plot. Sub-picosecond mean-squared displacement is dominated by atomic vibrations, hence the steep slope from zero elapsed time to the first data point. Arrhenius plots showing the relationship between the average self-diffusion coefficients for two bulk systems and reciprocal temperature are presented in Fig. 2. The activation energies for self-diffusion of Si and O are 115 ± 3 and 114 ± 2 kcal/mol, respectively, over the temperature range 4800–7200 K. The mean self-diffusivity pre-exponential factors for Si and O

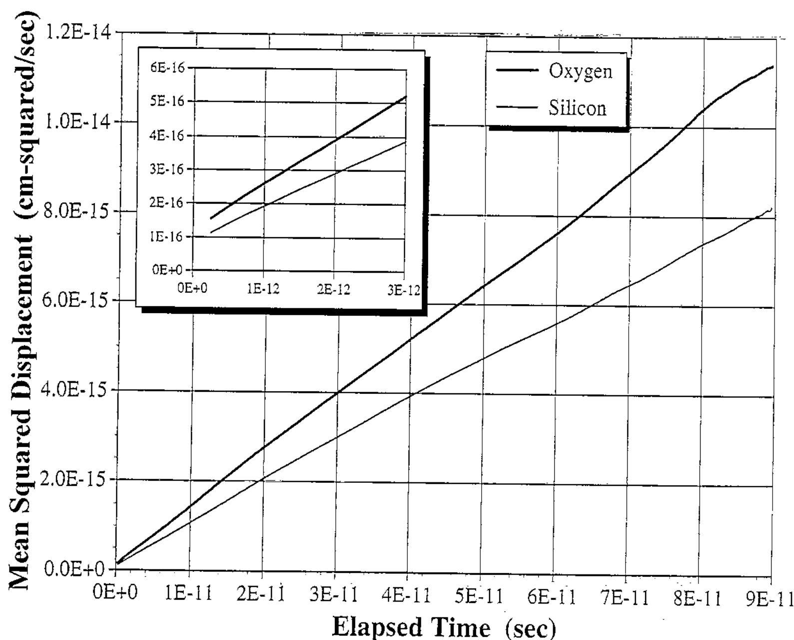

Fig. 1. Mean squared displacement as a function of time for oxygen and silicon atoms in bulk vitreous silica simulated at 6000 K.

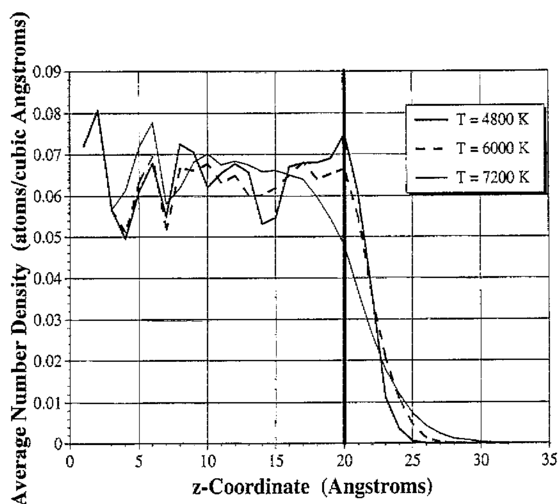

Fig. 3. Average number density as a function of z-coordinate for surface systems at 4800, 6000 and 7200 K. The vertical line indicates the cutoff used to define the surface for activation energy calculations, as discussed in the text.

are 0.21 and 0.26 cm^2/s, respectively. Including one standard deviation, the pre-exponential factors range from 0.17–0.27 and 0.22–0.32 cm^2/s, respectively, for Si and O.

3.2. Surface diffusion

Simulations of the vitreous silica surface show an increase in average diffusion coefficients of less than a factor of two over the bulk values for 3D, but close to a factor of 3 for 2D surface calculations. To calculate this surface diffusion coefficient, the mean-squared displacements of atoms with z-coordinates *continuously* above a specified value were averaged over all elapsed times, Δt, for which this condition was met. The z-cutoff was chosen such that the region above the cutoff had a lower average atomic density than the bulk. The density profiles of a surface system at 4800, 6000 and 7200 K are shown in Fig. 3. Average atomic density decreases from the bulk average to zero over 5–10 Å, depending on the temperature. An atomistic representation of the density profile of the surface is presented in Fig. 4, which models a typical surface configuration at 6000 K. Fig. 4(a–c) are sighted down the z-axis of the system (top view), and show atoms with z-coordinates higher than 18, 20, and 21 Å, respectively. Fig. 4(d–f) are sighted down the y-axis of the system (side view), using the same cutoffs as in Fig.

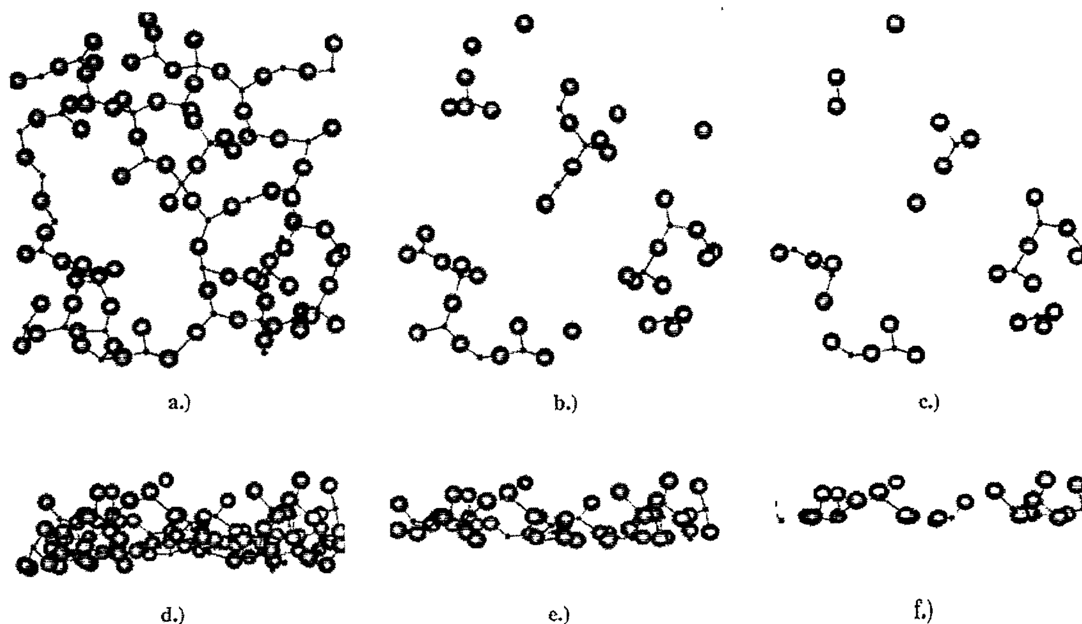

Fig. 4. Atomistic representation of the change in number density moving from the bulk to the surface for a typical silica surface configuration at 6000 K; (a–c) are sighted down the z-axis, (d)–(f) are sighted down the y-axis, (a, d) show all atoms above 18 Å, (b, e) show atoms above 20 Å and (c, f) show atoms above 21 Å.

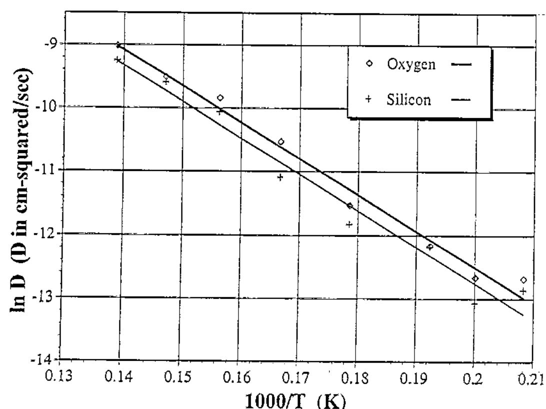

Fig. 5. Arrhenius plot of the natural log of D for Si and O in silica surface simulations as a function of reciprocal temperature for atoms that remain above a 20 Å cutoff for the last 9 ps of the 10 ps run.

4(a–c). Surface roughness of several angstroms is apparent in Fig. 4.

Fig. 5 is an Arrhenius plot of the average 3D diffusion coefficients of three surface systems. Mean-squared displacements were calculated for atoms in the region represented by Fig. 4(b) and (e). The > 20 Å cutoff used is indicated by the vertical line in Fig. 3. The diffusion coefficient was taken from the slope of the $\bar{r}^2$ versus t curve prior to any large jumps in the slope caused by a few highly diffusive surface atoms, as discussed in detail later with respect to Fig. 10. The mean activation energies virtually matched the bulk values, at 113 kcal/mol for both species. Mean diffusivity pre-exponential factors were 0.26 cm^2/s for Si and 0.33 cm^2/s for O using $\alpha = 3$ (3D diffusion, as shown in Fig. 10), approximately 20% higher than the bulk values or 0.39 cm^2/s and 0.50 cm^2/s for Si and O, respectively, for 2D diffusion ($\alpha = 2$).

4. Discussion

4.1. Bulk diffusion

The present simulation result for bulk diffusion at 6000 K is less than half that found in the simulation data of Woodcock et al. [21] who reported self-diffusivity values of $5 \pm 0.5 \times 10^{-5}$ cm^2/s for both species, while a value of 2×10^{-5} cm^2/s was found in our simulations. The Soules [19,20] simulation data extrapolate to values one to two orders of magnitude lower than those of the present work. Table 1 lists activation energy and diffusivity pre-exponential factor, D_0, data for several computational and experimental studies of bulk self-diffusion in SiO_2. The activation energies determined from Soules' published Arrhenius plots, 120 and 110 kcal/mol for Si and O, respectively, agree closely

Table 1
Activation energies (Q) and diffusivity pre-exponential factors (D_0) from simulation and experimental SiO_2 self-diffusion studies

Author	Q (kcal/mol)		D_0 (cm^2/s)		Temperature range (K)	Ref.
	Si	O	Si	O		
Present bulk average	115 ± 3	114 ± 2	0.17–0.27 mean: 0.21	0.22–0.32 mean: 0.26	4800–7200	–
Present surface averages	113 ± 7	113 ± 6	3D: 0.14–0.49 3D mean: 0.26 2D: 0.27–0.62 2D mean: 0.39	3D: 0.20–0.55 3D mean: 0.33 2D: 0.37–0.72 2D mean: 0.50	4800–7200	–
Soules	120 [a]	110 [a]	0.009 [a]	0.01 [a]	8000–20000	[19]
Kubicki and Lasaga	110 [a]	120 [a]	0.18 [a]	0.45 [a]	6000–8000	[17]
Mikkelsen	–	108.4	–	2.6	1473–1673	[10]
Brebec et al.	138	–	328	–	1383–1683	[11]
Hetherington et al.	122–170 [b]		–	–	1173–1673	[12]

[a] Calculated from Arrhenius plots given in the references.
[b] Activation energies for viscous flow determined by fiber elongation experiments on several commercial glasses.

with those of the present work, though he reported higher values of 140 kcal/mol. As shown in Table 1, diffusivity pre-exponential factors more than an order of magnitude lower than those of the present work account for Soules' lower extrapolated diffusion coefficients.

Kubicki and Lasaga [17] reported diffusion data which showed a change in activation energy as temperature decreased. The high temperature activation energy was approximately 110 and 120 kcal/mol for Si and O, respectively, for 6000 to 8000 K simulations and approximately 25 kcal/mol for both 2500 to 6000 K simulations. However, these data are questionable due to the short simulation times used. Root-mean-squared displacements calculated from their reported diffusion coefficients over the run times that they used were lower than 0.5 Å. Thus thermal vibrations rather than diffusive events account for the majority of atomic displacement for these data.

Experimental self-diffusion data for O and Si in v-SiO_2 after Mikkelsen [10] and Brebec et al. [11], respectively, are shown in Fig. 6. Comparing these data, oxygen self-diffusion coefficients were between one and two orders of magnitude higher than those for silicon over this range of temperatures. Mikkelsen reported an oxygen activation energy of 108.4 kcal/mol and a pre-exponential factor, D_0, of 2.6 cm^2/s. Brebec et al. determined a silicon activation energy of 138 kcal/mol and a D_0 of 328 cm^2/s. As shown in Table 1, the differences in Si and O

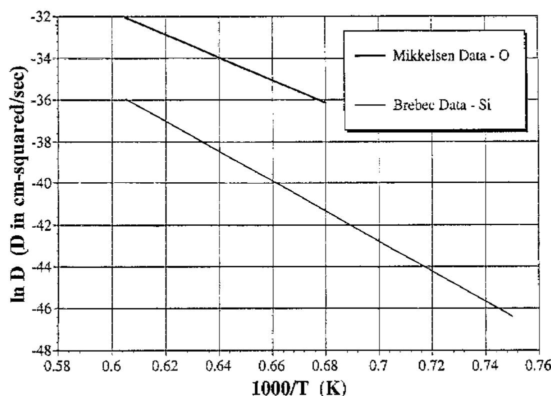

Fig. 6. Arrhenius plot of experimental data determined from concentration profiles of isotope tracer-doped diffusion couples. Oxygen data is from Ref. [10], silicon data from Ref. [11].

diffusivity data are in contrast to the present and previous simulations [17,19–21,30] which indicate approximately equal activation energies for Si and O self-diffusion and slightly higher O pre-exponential factors than Si pre-exponential factors.

Since Mikkelsen and Brebec et al. used different types of v-SiO_2 as substrates in their respective experiments, the simulations suggest that the differences in activation energies and pre-exponential factors found in the experiments were due to different impurities in the substrates. This hypothesis is supported by fiber elongation viscosity measurements of glasses similar to those used in the diffusion experiments, reported by Hetherington et al. [12]. The substrates used in Brebec et al.'s study were electrically fused quartz whereas those used in Mikkelsen's study were vapor-phase deposited amorphous silica. Although no chemical analyses of the diffusion substrates were reported, electrically fused quartz tends to have higher concentrations of metallic impurities and lower hydroxyl concentration than vapor-phase deposited amorphous silica, as discussed by Hetherington. Hetherington [12] found that the activation energy for viscous flow decreased with increasing hydroxyl concentration. Thus, the amorphous silica used in Mikkelsen's study should show lower activation energy for self-diffusion than the fused quartz used in Brebec et al.'s study, to be consistent with Hetherington's data. This is indeed the case. Hetherington also showed that increasing the metallic impurity content has little effect on the activation energy, but decreases the viscosity pre-exponential factor, η_0. The Arrhenius relation for the temperature dependence of viscosity, η, is

$$\eta = \eta_0 \exp(+Q/RT), \tag{6}$$

where Q is the activation energy for viscous flow and R is the ideal gas constant. Reduction of η_0 with no change in Q corresponds to lower viscosity and thus higher mobility. Higher mobility with no change in activation energy thus corresponds to higher diffusivity pre-exponential factor, D_0, according to Eq. (5). The presumably higher metallic impurity content of the electrically fused quartz substrates of Brebec's study should result in higher D_0 to be consistent with the viscosity study. Again, this is the case.

Thus the variation in the experimental activation energies and pre- exponential factors for Si and O bulk self-diffusion may be an extrinsic effect caused by the presence of different impurities in each glass. Hetherington [12] reported that activation energies for viscous flow varied between 122 and 170 kcal/mol depending on hydroxyl and metal impurity content. The Brebec et al. data showed close agreement between viscosities calculated from the diffusion coefficients by the Stokes–Einstein relation and experimental viscosities of the same glass used in the diffusion experiment [11]. This suggests that the mechanism for self-diffusion is similar to that for viscous flow. The simulation and experimental self-diffusion and viscous flow activation energies listed in Table 1 are in reasonable agreement with the average Si–O bond energy of 110 kcal/mol. This indicates that these mechanisms are activated by a single Si–O bond break.

Differences in pre-exponential factor can be understood in terms of the random-walk diffusion theory which gives the following relation for the diffusivity pre-exponential factor:

$$D_0 = \gamma a_0^2 \nu \exp(\Delta S/R), \quad (7)$$

where γ is a geometrical constant, a_0 is the jump distance, ν is the jump frequency, and ΔS is the change in entropy. The slight difference in the simulation Si and O pre-exponential factors can be attributed to different jump distances. As discussed above, differences between the experimental Si and O pre-exponential factors can be attributed to different impurity content. The one to three order of magnitude difference between the simulation and experimental pre-exponential factors indicates that the experimental data overestimates the entropic contribution to self-diffusion because of the impurity effect (or the simulation underestimates it), since only the exponential term in Eq. (7) could account for differences of orders of magnitude.

Several other investigators have reported oxygen self-diffusion data in vitreous silica [2–9], as reviewed by Lamkin et al. [1]. Their experiments involved exchange between gaseous $^{18}O_2$ and silica substrates. Generally, both oxygen network self-diffusion and molecular oxygen interstitial diffusion data were reported in these studies. In comparison to the diffusion couple and simulation data discussed above, both the activation energies and pre-exponential factors for self-diffusion were much lower. Activation energies ranged from 20–35 kcal/mol, while pre-exponential factors were between 10^{-11} and 10^{-9} cm^2/s. As discussed by Lamkin et al., the activation energies reported for self-diffusion in these studies were similar to that for molecular oxygen diffusion in silica, 27 kcal/mol. This suggests that the mechanism for the self-diffusion observed in these studies is controlled by the presence of the gaseous oxygen, which is absent in Mikkelsen's diffusion couple experiment and the present simulations.

Brawer has described diffusive mechanisms observed in molecular dynamics simulations of BeF_2 glasses, which are network glasses analogous to v-SiO_2. He stated that diffusion occurs by the creation of overcoordinated ion defect sites, followed by the breakup of these defects such that some ions change neighbors [25,26]. Similar mechanisms were observed in the present simulations.

The simulations show that when one of the Si–O bonds breaks at an overcoordinated defect, the geometry surrounding the central species changes. This carries the central species away from the newly formed undercoordinated defect. When a site becomes available, the undercoordinated species completes its diffusive jump. Often this is accomplished by forming another overcoordinated defect, thus propagating a chain reaction. Si–O bonds that break between stoichiometrically coordinated species usually reform since the change in bonding geometry is insufficient to carry either species away from the other.

Diffusive jumps in a bulk glass at 6000 K by an oxygen atom released from a five-coordinate silicon atom and a silicon atom debonding from a three-coordinate oxygen atom are shown in Figs. 7 and 8, respectively. In part (a) of both of these figures, the silicon and oxygen atoms of interest are labeled and are represented by the two largest spheres. The smallest spheres represent silicon atoms, while the small lighter shaded spheres represent oxygen atoms. Only the tetrahedra that participate in neighbor exchange are shown but these tetrahedra are connected to the rest of the glass via siloxane bonds not drawn. The numbering schemes are explained forthwith. As depicted in Fig. 7(a), the coordination polyhedron around the five-coordinated Si defect (Si(1)) is ob-

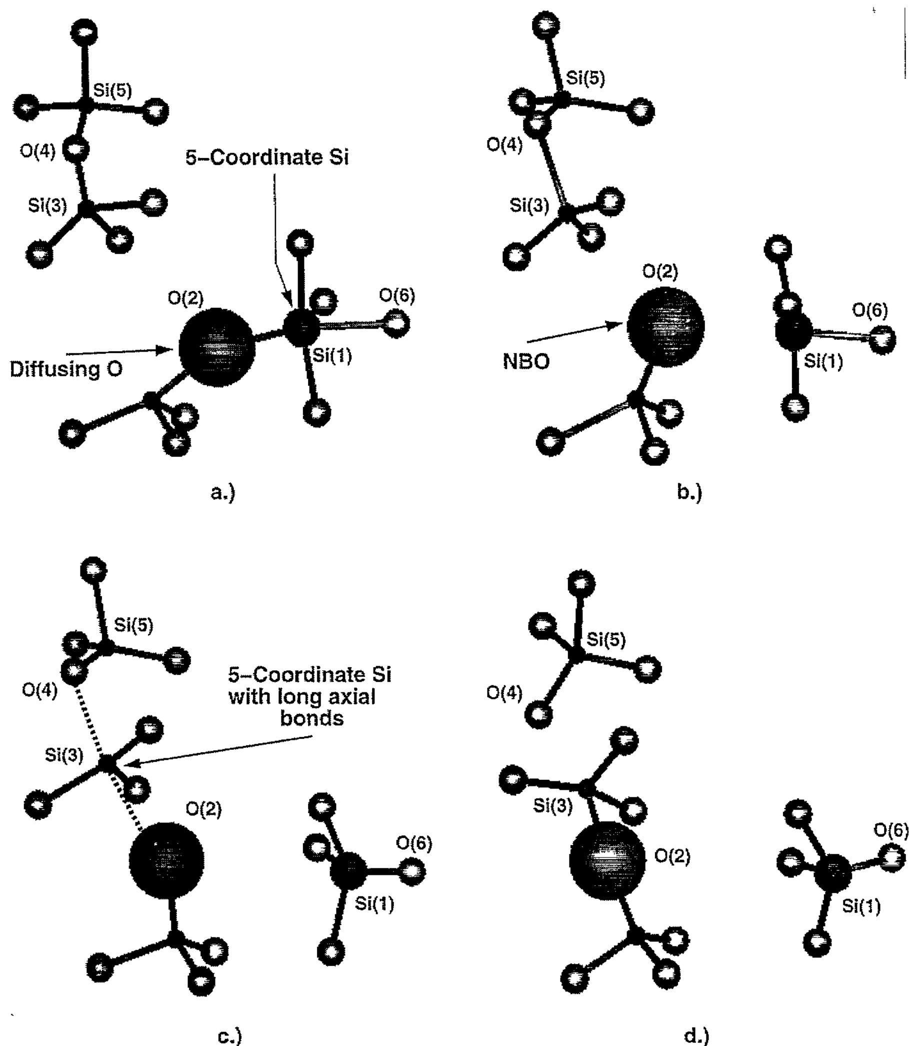

Fig. 7. Diffusive jump of an oxygen atom (O(2)) originally bonded to a five-coordinate silicon atom (Si(1)) in a bulk glass at 6000 K. See description in text.

served to have trigonal-bipyramidal geometry, with three coplanar Si–O bonds and two axial bonds perpendicular to them. In Fig. 7(b), the diffusing oxygen (O(2)) is released from Si(1) via a bond rupture. At the same time, there is an Si–O bond elongation between Si(3) and its bridging oxygen connection (O(4)) to Si(5). In coordinated behavior, Si(1) moves to the right to shorten the axial bond to O(6) while its planar oxygens relax to accommodate tetrahedral symmetry around Si(1). This reduces the attraction of O(2) to Si(1). Concurrently, Si(3) continues its motion away from O(4) and forms, in Fig. 7(c), a trigonal bipyramidal structure with two very long axial bonds (indicated by dashed lines) to O(2) and O(4). Fig. 7(d) shows completion of O(2)'s move to Si(3) (and vice-versa), thus completing the diffusive jump. Interestingly, these reactions are very similar to those observed in our simulations of sol–gel polymerization using silicic acid molecules [32]. However, in the sol–gel work, H ions were present which influenced the reaction mechanism.

As shown in Fig. 8(a), three-coordinate oxygen defects exhibited trigonal planar geometry, with three coplanar Si–O bonds and Si–O bond angles at ap-

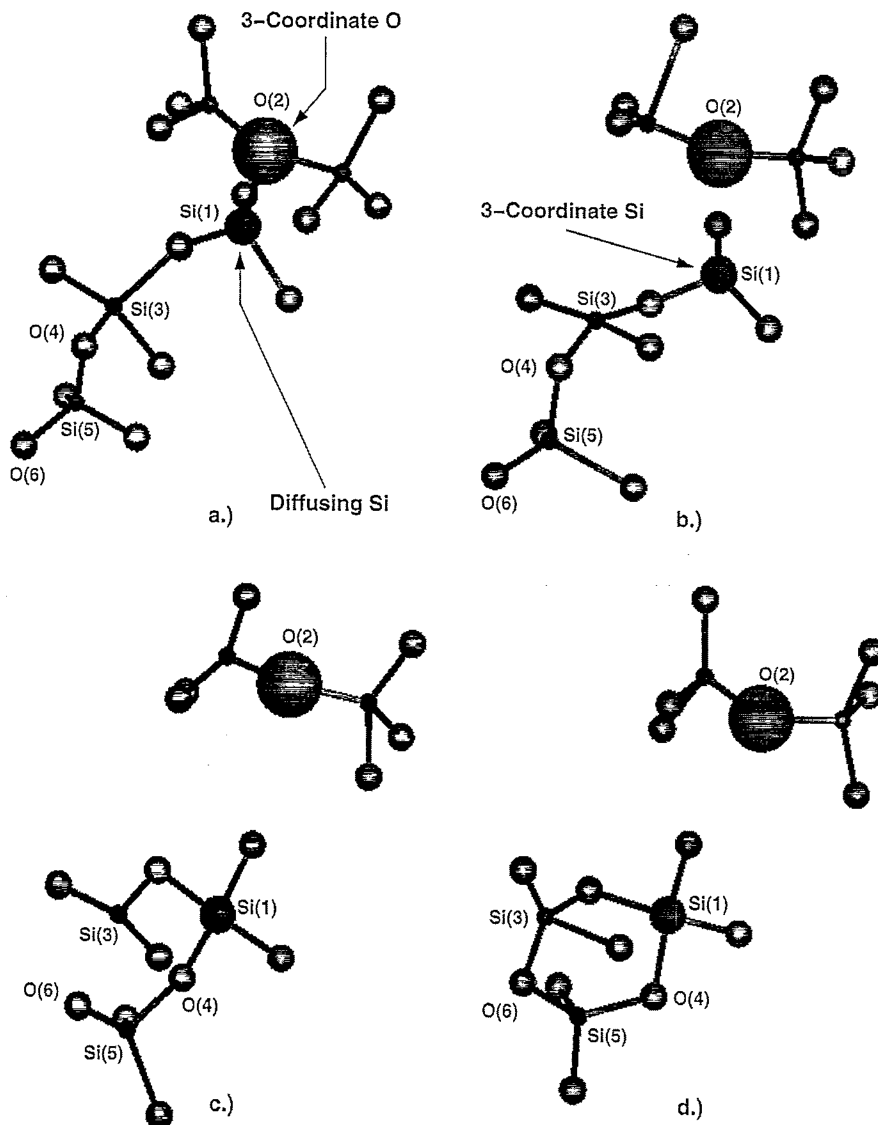

Fig. 8. Diffusive jump of a silicon atom (Si(1)) originally bonded to a three-coordinate oxygen atom (O(2)) in a bulk glass at 6000 K. See description in text.

proximately 120°. Fig. 8(a) and (b) show the debonding of a silicon (Si(1)) from an overcoordinated oxygen (O(2)). While the remaining Si–O–Si bond angle around O(2) relaxes to approximately 150°, the undercoordinated silicon recoils into trigonal planar geometry. Again, the changes in coordination geometry resulted in a significant separation distance between the former nearest neighbors. Comparison of Fig. 8(b) and (c) shows that the tetrahedron around Si(5) rotates such that O(4) breaks its bond with Si(3) and forms a new bond in Fig. 8(c) with Si(1), returning Si(1) to four-coordination. The neighbor exchange is completed by the bonding of O(6) with Si(3), thus forming a three-membered ring (Fig. 8(d)).

Whereas Figs. 7 and 8 give examples of single diffusive jumps happening over a few picoseconds in the bulk glass, Fig. 9(a) and (b) show the initial and

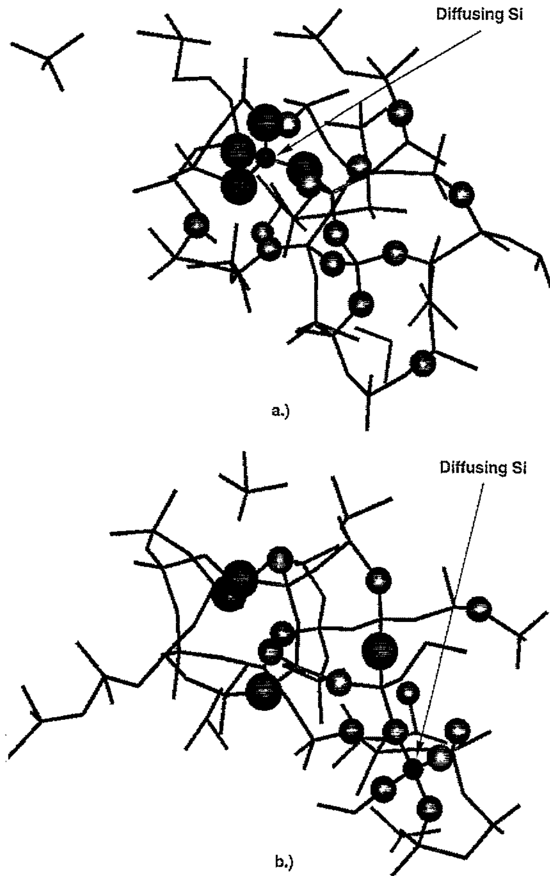

Fig. 9. Significant neighbor exchange occurs in the bulk glass at 6000 K after several diffusive jumps. Snapshot (b) is taken 12 ps after snapshot (a). (Small atom = diffusing silicon; medium atoms = oxygen atoms bonded to diffusing silicon at one time during 12 ps time evolution; large atoms = original oxygen neighbors in (a).)

final configurations of a 12 ps time evolution at 6000 K. Again the small sphere represents the silicon atom of interest, as labeled in Fig. 9(a). The largest, dark spheres are the nearest neighbor oxygen atoms bonded to the silicon during the initial configuration. The other large spheres represent all of the oxygen atoms that were bonded to this silicon at one time during the time evolution. Other silicon atoms are not shown, for clarity. As demonstrated by the number of oxygen atoms to which the diffusing Si becomes attached in the figure, significant neighbor exchange occurs as atoms diffuse in the bulk. None of the initial nearest neighbors of the diffusing silicon atom remained bonded to it after 12 ps (Fig. 9(b)). Single diffusive jumps usually involve only one neighbor exchange and thus could be viewed as rearrangement of tetrahedra and thus molecular diffusion. However, since significant neighbor exchange occurs, the long term behavior is similar to atomic interstitial or vacancy diffusion.

4.2. Surface diffusion

One difference between surface and bulk diffusion is that overcoordinated defects were not observed to be important precursors to diffusive jumps for surface self-diffusion since they are annealed out of the low density surface region at the temperatures studied. Tetrahedra with one or more NBO were seen to diffuse on breaking another Si–O bond by rotating around the remaining bridging bond(s). SiO_3 triangles with one or two NBO were also seen to form and rotate around the remaining bridging bond(s). Rotations of undercoordinated species result in larger jump distances than in the bulk due to the lower atomic density on the surface, which increases the distance between sites available for rebonding to the network. These larger jump distances account for the higher D_0 values (Eq. (7)) and thus higher diffusion coefficients (Eq. (5)) compared to bulk values.

Fig. 10(a–d) shows the rotation of an SiO_x polyhedron on the surface at 6000 K. Again, the silicon atom of interest is represented by the small dark sphere and is labeled in Fig. 10(a). The large dark spheres again represent the initial nearest neighbor oxygens to the Si atom in each of the figures. The lighter spheres again represent O atoms that bond to the Si at least once in the 12 ps time evolution. Other silicon atoms are not shown, for clarity. Fig. 10(a) and (b) show an SiO_4 tetrahedron with one NBO which exchanged neighbors on breaking one bridging bond and rotating around the two remaining bridges to a new site. Fig. 10(c) shows the atoms of interest after breaking two bonds to become an SiO_3 triangle with only one bond bridging it to the network. Although not shown in the figure, the SiO_3 triangle underwent very large scale vibrations for several picoseconds, sampling several oxygen atoms (shown as the smaller spheres) before finding a more stable site as shown in Fig. 10(d). Considerably less

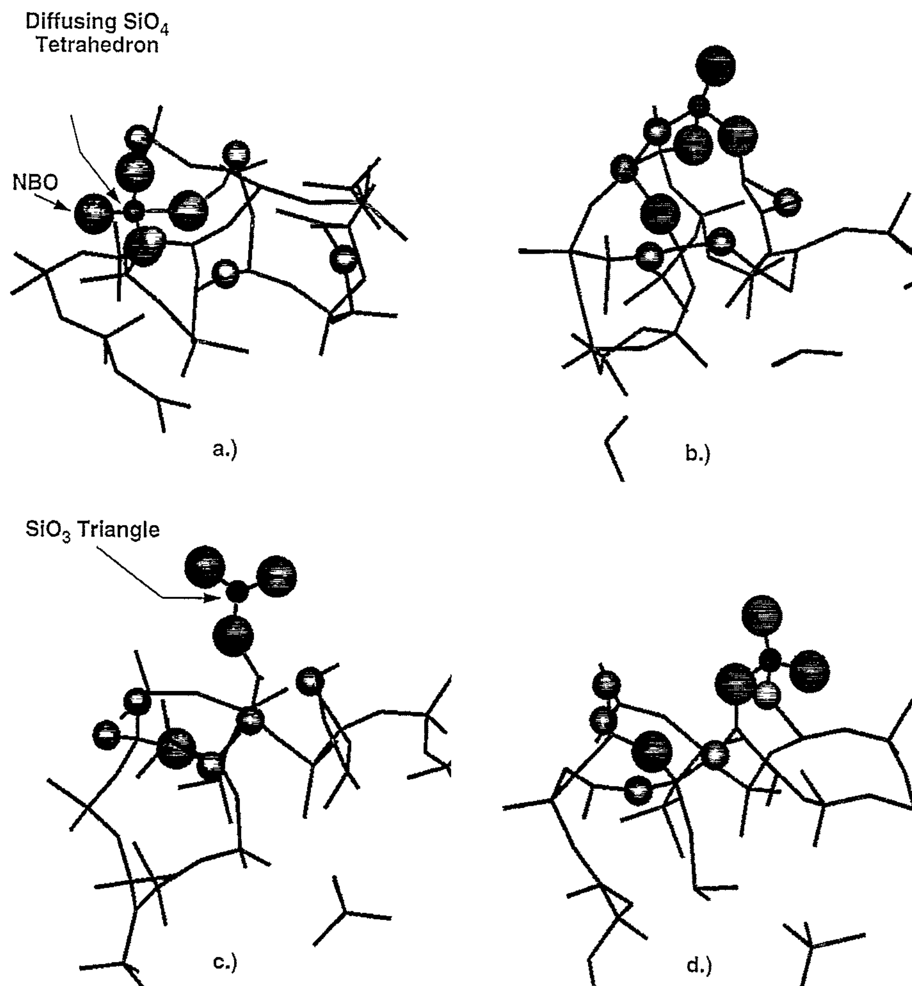

Fig. 10. Diffusing surface polyhedron at 6000 K. Snapshot (d) is taken 12 ps after snapshot (a). See description in text. (Small atom = diffusing silicon; medium atoms = oxygen atoms bonded to diffusing silicon at one time during 12 ps time evolution; large atoms = original oxygen neighbors in (a).)

neighbor exchange occurs during surface self-diffusion as compared to the bulk, as would be expected due to the lower atomic density in the surface region. This can be seen by comparing Figs. 9 and 10. More importantly, the outermost species on the surface which diffuse have access to the vacuum phase above the surface which affords easier rotational motion of clusters and larger jump distances.

The surprising result that diffusion coefficients in the lower atomic density surface region are only a factor of two or three higher than bulk diffusion coefficients can be understood by recognizing that in both environments, one Si–O bond must break to activate the process. This explains the match in activation energies between bulk and surface diffusion. The increase in diffusion coefficients for surface diffusion compared to bulk values is thus due to larger diffusivity pre-exponential factors, which are due to longer jump distances available in the surface region due to the presence of the free surface.

The residence time of individual atoms on the outer regions of the surface is quite small. Fig. 11 shows $\bar{r}^2$ as a function of Δt for oxygen diffusing above three different z-cutoffs at 6000 K. The higher z-cutoff indicates a thinner surface volume from which the displacement data are generated. The

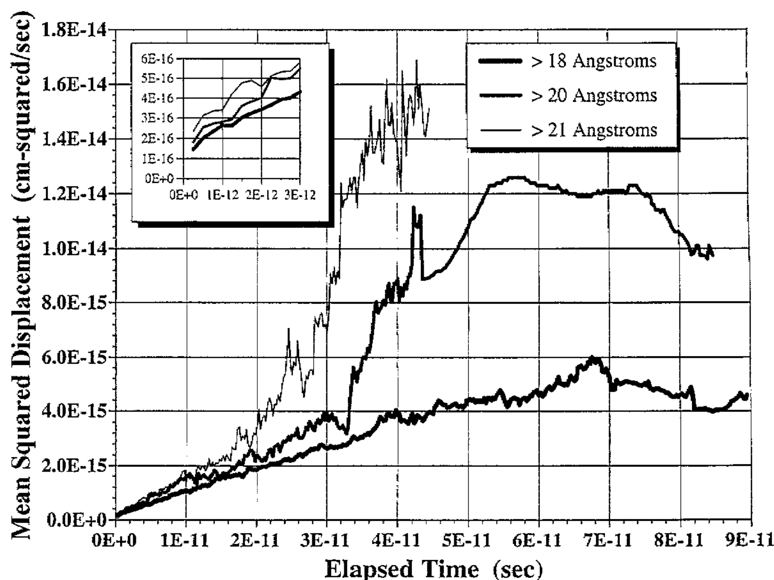

Fig. 11. Mean squared displacement for oxygen atoms on the surface at 6000 K. Data calculated from atoms that remain above a cutoff for the last 9 ps of the 10 ps run are shown for three different cutoffs.

elapsed time axis refers to time intervals, Δt, beginning at each configuration in the run, t_0, and ending at $t_0 + \Delta t$. For oxygen in the thickest surface volume slab (z-cutoff > 18 Å), the slope of the curve is relatively unchanged. However, with the thinner surface volumes, an abrupt change in the slope of oxygen displacement occurs above the cutoff of 20 Å at 3.3×10^{-11} s, while a similar abrupt change in slope occurs for oxygen which are above the 21 Å cutoff, but at a shorter elapsed time of 2.3×10^{-11} s. The abrupt changes in slope are caused by a few surface oxygen which have large displacements in the outer surface and which remain above the specified cutoff longer than other oxygen atoms. Since the number of these oxygens is small, they make a minor contribution to the data generated from the thickest volume shown in the figure (> 18 Å). However, as the surface volume which is sampled is thinned, the number of oxygen which remain in the slab for longer times is decreased, resulting in an increased effect of those oxygen showing large displacements.

If we consider the abrupt change in the slope of the curve to be an upper limit on the average residence time of the oxygen in the specified surface volume, Fig. 11 shows that this residence time decreases by about 10 ps as the cutoff is raised one angstrom (from oxygen above 20 Å to those above 21 Å). Clearly, atoms in the outer surface region diffuse a few angstroms in the z-direction. However, the atoms contributing to the high slope region of the > 20 and > 21 Å curves in Fig. 11 are clearly diffusing primarily in the x- and y-directions, otherwise they would not have remained above the cutoff continuously for much longer times than the average. Thus mechanisms for surface diffusion at much higher rates than in the bulk average do operate, but not in sufficient quantities to dominate the short-time average coefficients determined using a cutoff. The SiO_3 triangle in Fig. 10(c) is an example of a defect that diffuses primarily in the x- and y-directions. Analysis of several similar high diffusion rate events indicate diffusion coefficients an order of magnitude higher than in the bulk. Activation energies are again similar to the bulk, while pre-exponential factors are an order of magnitude higher.

Therefore, depending upon the thickness of the surface volume parallel to the free surface used to generate the diffusion data, diffusion coefficients similar to or fairly different from those generated in the bulk of the glass can be obtained. This shows that mechanisms enabling large displacements at the outermost surface of the glass exist, but that displacements fairly similar to bulk behavior dominate a few angstroms below the surface.

In addition to this high-rate surface diffusion, individual oxygen and SiO_3 molecules were seen to evaporate from the surface at the four higher temperatures studied. The displacements of these evaporated species were not included in the diffusion coefficient analyses. At the two highest temperatures, 6800 and 7200 K, this mechanism does appear to be important as several atoms evaporate then condense after large displacements.

The discussion presented above regarding the difference between average bulk and surface self-diffusion coefficients in perfect vacuum suggest that the presence of a solid (or even liquid) interfaced with the silica surface could change the mechanism by which silicon and oxygen atoms diffuse at the outermost surface.

5. Conclusions

The activation energy for self-diffusion in simulated bulk vitreous silica was found to be 115 kcal/mol for both Si and O, in reasonable agreement with data from diffusion-couple tracer experiments and previous simulations. Oxygen self-diffusion coefficients were less than a factor of two higher than those of silicon. This difference was manifested in the diffusivity pre-exponential factors, D_0, which were 0.26 cm^2/s for O and 0.20 cm^2/s for Si. The self-diffusion activation energies are similar to that for viscous flow, suggesting that the mechanisms are similar. Overcoordinated defects were observed to be important precursors to diffusive jumps.

Surface diffusion coefficients were found to be larger than those of bulk simulations by a factor of ~ 2 for the thicker surface volumes, and as much as an order of magnitude higher for the thinnest surface volume. Activation energies for surface self-diffusion were very similar to those of the bulk. Surface diffusivity pre-exponential factors approximately 20% higher to an order of magnitude higher than bulk values accounted for the higher surface diffusion coefficients. As in the bulk, surface diffusion is activated by a single Si–O bridging bond breaks. Small numbers of species diffusing on the surface with only one bridging bond to the network were observed; these species exhibited diffusion coefficients approximately an order of magnitude higher than bulk values. However, these species did not occur in sufficient numbers to significantly affect the average surface diffusion coefficients obtained from thicker surface volumes.

References

[1] F.L.R. Lamkin, R.J. Fordham, J. Eur. Ceram. Soc. 10 (1992) 347.
[2] J.D. Cawley, R.S. Boyce, Philos. Mag. A58 (1988) 589.
[3] S.S. Cristy, J.B. Condon, J. Electrochem. Soc. 128 (1981) 2170.
[4] C.J. Han, C.R. Helms, J. Appl. Phys. 59 (1986) 1767.
[5] M.I. Heggie, Philos. Mag. Lett. 65 (1992) 155.
[6] M.I. Heggie, R. Jones, C.D. Latham, S.C.P. Maynard, P. Tole, Philos Mag. B65 (1992) 463.
[7] J.D. Kalen, R.S. Boyce, J.D. Cawley, J. Am. Ceram. Soc. 74 (1991) 203.
[8] K. Muehlenbachs, H.A. Schaeffer, Can. Mineral. 15 (1977) 179.
[9] J. Rodriguez-Viejo, F. Sibieude, M.T. Clavaguera-Mora, C. Monty, Appl. Phys. Lett. 63 (1993) 1906.
[10] J.C. Mikkelsen Jr., Appl. Phys. Lett. 45 (1984) 1187.
[11] G. Brebec, R. Seguin, C. Sella, J. Bevenot, J.C. Martin, Acta Metall. 28 (1980) 327.
[12] G. Hetherington, K.H. Jack, J.C. Kennedy, Phys. Chem. Glasses 5 (1964) 130.
[13] S.S. Mann, T. Seto, C.J. Barnes, D.A. Kin, Surf. Sci. 261 (1992) 155.
[14] H.H. Rotermund, Surf. Sci. 283 (1993) 87.
[15] B.P. Feuston, S.H. Garofalini, J. Chem Phys. 89 (1988) 5818.
[16] S.H. Garofalini, J. Chem. Phys. 76 (1982) 3189.
[17] J.D. Kubicki, A.C. Lasaga, Am. Mineral. 73 (1988) 941.
[18] S.K. Mitra, Philos. Mag. B45 (1982) 529.
[19] T.F. Soules, J. Non-Cryst. Solids 49 (1982) 29.
[20] T.F. Soules, J. Non-Cryst. Solids 123 (1990) 48.
[21] L.V. Woodcock, C.A. Angell, P. Cheeseman, J. Chem. Phys 65 (1976) 1565.
[22] P. Vashishta, R.K. Kalia, J.P. Rino, I. Ebbsjo, Phys. Rev. B41 (1990) 12197.
[23] B. Vessal, M. Amini, D. Fincham, C.R.A. Catlow, Philos Mag. B60 (1989) 753.
[24] R.G. Della Valle, H.C. Andersen, J. Chem. Phys. 97 (1992) 2682.
[25] S.A. Brawer, J. Chem. Phys. 75 (1981) 3516.
[26] S.A. Brawer, Relaxation in Viscous Liquids and Glasses (American Ceramic Society, Columbus, OH, 1985).
[27] B.P. Feuston, S.H. Garofalini, J. Chem. Phys. 91 (1989) 564.
[28] B.P. Feuston, S.H. Garofalini, J. Appl. Phys. 68 (1990) 4830.
[29] S.H. Garofalini, J. Chem. Phys. 78 (1983) 2069.
[30] S.H. Garofalini, S. Conover, J. Non-Cryst. Solids 74 (1985) 171.
[31] R.L. Mozzi, B.E. Warren, J. Appl. Crystallogr. 2 (1969) 164.
[32] G.E. Martin, S.H. Garofalini, J. Non-Cryst. Solids 171 (1994) 68.